# Electron stimulated oxidation of the Ni(111) surface: Dependence on substrate temperature and incident electron energy

M. J. Stirniman, Wei Li, and S. J. Sibener
*Department of Chemistry and The James Franck Institute, The University of Chicago, Chicago, Illinois 60637*

(Received 14 December 1994; accepted 29 March 1995)

The effect of surface temperature on the rate of oxidation of the Ni(111) surface with and without electron irradiation has been determined for temperatures between 120 and 340 K. The oxidation rate in the presence of an electron beam demonstrates an inverse dependence on the substrate temperature, while without an electron beam we observe a decrease in oxidation rate with decreasing substrate temperature, decreasing almost to zero at 120 K. Similar rates are observed near room temperature for the two cases. We have found that oxidation of this surface can be well described by either of two rate expressions: one that relates the oxide growth rate to the rate of lateral growth of two dimensional oxide islands, and another that is first order in oxide and oxygen coverages at the surface. The physical implications of each model are discussed in terms of the nucleation sites created by the electron beam, and the rate constants for oxidation at these nucleation sites. We present evidence that the nucleation sites created by the electron beam are metastable, with an unusually long half-life of about $600 \pm 150$ s. We have also investigated the dependence of the cross section for nucleation center creation as a function of incident electron energy at constant electron flux and constant oxygen exposure. The energy dependencies of the cross section for nucleation center creation and the yield of secondary electrons produced by irradiation from the incident electron beam are compared, leading to consideration of the role that such secondary electrons may have in the creation of nucleation centers. The results presented herein delineate the correct low temperature oxidation kinetics for Ni(111) in the absence of perturbing electrons. They also provide a cautionary note for experiments which use electron-based probes, or optical probes which generate intense swarms of electrons, for studying the oxidation kinetics of metals, and perhaps other classes of interfacial reactions. 

## I. INTRODUCTION

The corrosion of materials is a subject of the most fundamental importance, from both the standpoints of basic research and of technological development. Among corrosion processes, the oxidation of metals is perhaps the most widely studied, due to its significance in real world applications.

A great deal is known about the initial stages of oxidation of nickel surfaces due to work by a number of authors,[1–3] most notably Holloway and Hudson.[4,5] In a recent paper, a reinvestigation of the $O_2$/Ni(111) system reported the observation of a marked synergistic effect in the oxidation of this surface at low temperature and under irradiation from an electron beam.[6] Subsequent work in our laboratory using high resolution electron energy loss spectroscopy (HREELS) further characterized this effect.[7] Upon review of the literature, it appears that most earlier studies of this system were done using either low energy electron diffraction (LEED) or Auger spectroscopies as experimental probes, conditions that we have shown result in a greatly increased rate and extent of oxidation at low temperatures ($<200$ K).[6,7] While these earlier studies unfortunately did not address the true oxidation process of low temperature nickel surfaces, they do (unintentionally) provide much useful information on the electron beam stimulated oxidation of these surfaces.

The uptake of oxygen on the low temperature electron irradiated Ni(111) surface proceeds in three distinct regions. First is a rapid uptake of oxygen to an initial coverage of about 0.4 ML chemisorbed O. This initial uptake is fairly independent of temperature or the presence of electron irradiation, and can be well described by a first order dissociative adsorption rate expression.[4] This is followed by a second rapid uptake region, associated with the nucleation and growth of nickel oxide, which demonstrates an inverse dependence of the reaction rate on the substrate temperature. The third region is a very slow thickening of the saturated nickel oxide overlayer, which is also insensitive to substrate temperature in the temperature regime explored and insensitive to the presence of electron irradiation. In contrast, oxygen uptake on this surface without electron irradiation follows the same three-step pattern, but with an opposite substrate temperature dependence on the reaction rate in the second region,[6,7] i.e., it exhibits normal behavior for a thermally activated process. The present kinetic study is concerned with this second region, the nucleation and growth of nickel oxide from the saturated chemisorbed overlayer to the saturation coverage of nickel oxide, both with and without electron irradiation.

To summarize our work to date, in Ref. 6 we have previously shown that at 120 K, and without electron irradiation, oxygen dissociatively adsorbs on the Ni(111) surface to a saturation coverage of only about 0.4 ML, followed by little or no subsequent oxygen adsorption. HREELS spectroscopy was used to characterize the state of this oxygen overlayer, from which we concluded that this overlayer con-

sists almost exclusively of chemisorbed oxygen. However, in the presence of an electron beam at 120 K, oxygen again quickly adsorbs to the saturation coverage for chemisorption, but in contrast to the above case, is followed by rapid oxide nucleation and growth to the saturation oxide coverage. The thickness of the saturated oxide layer at room temperature and below is generally taken to be three layers of NiO.[1] Using a rate expression that was first order in both the oxide coverage and the nucleation site density, we were able to fit oxygen uptake vs electron beam flux curves at constant oxygen exposure. These curves were fit with only one parameter, the (energy-dependent) cross section for the creation of nucleation sites by the electron beam. The cross sections that were extracted from the fits to the incident electron beam energy data (ca. $5\times10^{-18}$ to $3\times10^{-17}$ cm$^2$) are similar to the cross sections for a wide variety of electron beam stimulated surface effects, including dissociation,[8] desorption,[9] and migration.[10] With the cross sections thus obtained, this kinetic model was also able to quantitatively predict oxygen uptake vs oxygen exposure curves at constant electron flux. We wish to stress that the electron beam effect that we have observed, while evident to a small degree at room temperature and above, is most dramatic at temperatures below about 200 K.

Complementing this study, the investigation of the oxidation of this surface using HREELS has shown that the low incident flux (ca. 2.5 nA cm$^{-2}$) and energy (7 eV) of the electron beam from the HREELS monochromator to be a suitable probe of oxygen interaction with this surface.[7] Our HREELS spectrometer allowed nonperturbative monitoring of the amount of oxygen uptake, through the intensity of the loss peak due to chemisorbed and oxidized oxygen. In addition, this method can be used to characterize the chemical nature of the oxygen species during the oxidation process, through the shifts in the energy of the oxygen loss peak.

In the present work we present a careful reinvestigation of the kinetics of the oxidation of the Ni(111) surface. Using both a kinetic expression related to the rate of oxide island growth as developed by Holloway and Hudson,[4] and an autocatalytic rate expression derived from an extension of our earlier model, we fit oxygen uptake vs exposure curves for both electron assisted oxidation and nonassisted oxidation. We determine the correct rates for the oxidation of this surface without electron irradiation for each of the models, leading to the determination of activation energies, and discuss the effect of the electron beam on the oxidation process in terms of the parameters obtained from fitting the models to the data. We provide evidence that the nucleation sites created by the electron beam are metastable, and fit their disappearance rate with a simple exponential with a half-life of about 10 min. In addition, we report a more detailed investigation of the dependence of the cross section for electron creation of nucleation centers on the incident electron energy in the range of 30 to 2000 eV.

These findings are important as they delineate the correct rates for metallic oxidation at low temperatures in the absence of the perturbative effects of electron irradiation. Moreover, the synergistic influence that electrons have on this oxidation process and the associated large cross sections for this effect suggest possible new methodologies for scanning tunneling microscopy and scanning electron microscopy based lithographies.

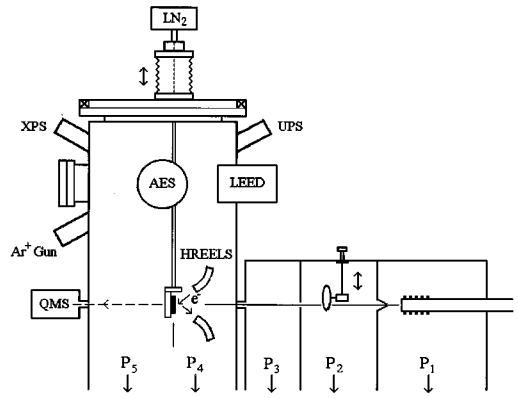


FIG. 1. Schematic diagram of the combined molecular beam/inelastic electron scattering apparatus. The ion/Ti sublimation/turbomolecularly pumped UHV chamber has a large rotating lid which transports the (off-center mounted) manipulator to various experimental positions. Level 1 is for scattering and HREELS measurements (electron optics shown 90° rotated from actual orientation for presentation purposes), while level 2 is for electron irradiation and surface preparation. The triply differentially pumped molecular beamline ($P_1$,$P_2$: diffusion pumps, $P_3$: turbomolecular pump) has a heated supersonic nozzle beam source which is skimmed before entering the beam modulation chamber; short-pulse time-of-flight, square-wave (50% duty cycle) chopping, and cross-correlation modulation patterns are available. Not shown: double layer of magnetic shielding which encloses the electron spectrometer.

## II. EXPERIMENT

The experiments were carried out in a two level UHV system, shown schematically in Fig. 1, that has been described previously.[11] Briefly, the upper level of the chamber is equipped with a double-pass cylindrical mirror Auger spectrometer, LEED optics, and a sputter ion gun. The lower level contains an HREELS spectrometer and a three-fold differentially pumped supersonic molecular beam source. The beam source geometry is such that the molecular beam strikes the crystal at the focus of the electron beam of the HREELS monochromator (Fig. 1). The chamber is pumped by a 300 1s$^{-1}$ ion pump, a liquid nitrogen cooled titanium sublimation pump, and a 60 1s$^{-1}$ turbomolecular pump. The ultimate pressure is less than $8\times10^{-11}$ Torr as measured by an ion gauge in the upper level of the chamber, and less than $4\times10^{-11}$ Torr as measured near the inlet of the ion pump. A Ni sample oriented along the $\langle111\rangle$ direction to within 0.2° was used for the present work. The crystal was prepared by repeated cycles of $Ar^+$ sputtering followed by annealing to 1100 K. The sample could be cooled with liquid nitrogen to 110 K and heated by electron bombardment of the back of the crystal to 1300 K, with heating to 350 K and below accomplished by radiative heating of the back of the sample in combination with liquid nitrogen cooling. Temperatures were measured with a type K thermocouple spot welded to the side of the crystal, and were controlled to within 0.1 K with a Eurotherm temperature controller. The electron assisted oxidation data were obtained by backfilling the cham-

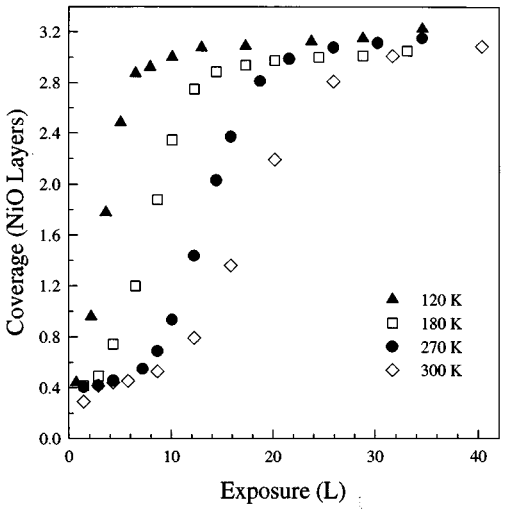


FIG. 2. Extent of oxidation vs exposure curves for electron stimulated oxidation at four substrate temperatures. The curves exhibit the three characteristic stages of oxygen uptake: an initial fast chemisorption region up to the equivalent of about 0.4 layers NiO (not shown here), an oxide nucleation induction period, and finally the growth of oxide up to a saturation thickness of 3 layers NiO. Note the inverse dependence of the oxidation rate on the substrate temperature.

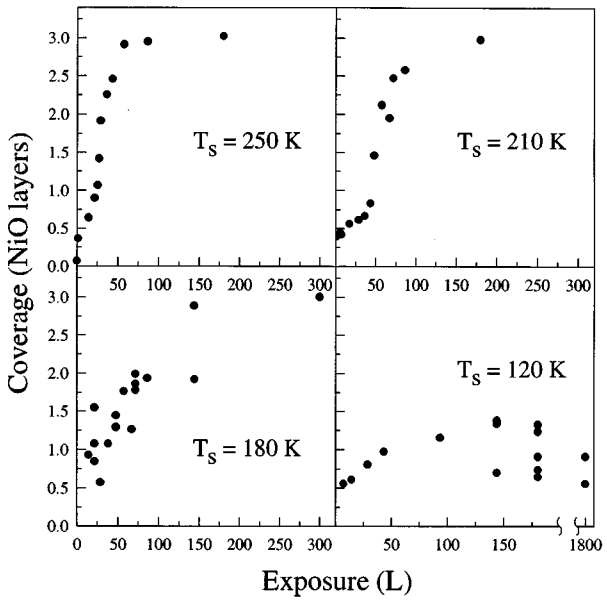


FIG. 3. Extent of oxidation vs exposure curves for oxidation without electron stimulation, over a similar range of substrate temperatures as shown in Fig. 2. The overall rate of oxidation in this case decreases with decreasing substrate temperature, in contrast to the temperature dependence for electron stimulated oxidation. Also note that the fastest oxidation rate shown here is still much slower than the electron assisted data at 120 K (Fig. 2).

ber with oxygen to an uncorrected ion gauge reading of $3\times10^{-8}$ Torr, while irradiating the sample with a 2 keV electron beam from the electron gun of the Auger spectrometer at an electron flux of 2.00 mA $cm^{-2}$. The peak-to-peak heights of the oxygen 508 eV and nickel 848 eV derivative Auger lines were recorded periodically during dosing. The recording of a single Auger spectrum took approximately 12 s, and typical time to collect an oxygen uptake vs exposure curve was 1500 s. The oxygen uptake curves for nonelectron assisted oxidation were obtained using $O_2$ pressures from $3\times10^{-8}$ to $3\times10^{-6}$ Torr.

## III. RESULTS

### A. Temperature dependencies

Figure 2 shows representative oxygen uptake vs exposure curves for electron stimulated oxidation at several substrate temperatures. The vertical scale is layers of NiO, converted from oxygen Auger intensities as in Ref. 4. To minimize uncertainties due to variations in our Auger spectrometer, we always measured the ratio of oxygen 508 eV to nickel 848 eV Auger peak-to-peak intensities, and periodically checked that the saturation coverage of NiO resulted in a consistent value of the Auger ratios. The horizontal axis is units of exposure in Langmuirs ($1\ L=10^{-6}$ Torr s). The shape and temperature dependence of these curves agree quantitatively with uptake curves of other authors for oxidation of Ni(111),[5,12] and are also in good agreement with oxidation curves for Ni(100).[3,4]

Figure 3 shows oxide growth vs surface temperature curves for a similar range of substrate temperatures as in Fig. 2, but without electron irradiation. The scatter in these data is primarily a result of the experimental method of measurement. To avoid exposing the oxygen overlayer to an electron beam before or during dosing, each data point on a curve of oxygen uptake vs exposure required first exposing the sample to a certain amount of oxygen, followed by determination of the oxygen uptake with Auger spectroscopy, followed by a cleaning cycle of argon ion sputtering and annealing. A three step cleaning procedure, i.e., room temperature sputtering, followed by sputtering at 980 K, followed by annealing at 1100 K was always used to remove oxygen, whether it was chemisorbed or in an oxide. This was to prevent to accumulation of subsurface oxygen in the bulk of the nickel crystal, an effect that has been noted by a number of authors for Ni(111).[13–15] We attribute the scatter in the data to small variations in surface quality after each cleaning cycle. Despite the uncertainty, the oxide growth curves in Fig. 3 clearly show an opposite dependence of the oxidation rate on the substrate temperature than is the case for electron stimulated oxidation (Fig. 2). Furthermore, similar rates are observed for the two cases near 300 K, indicating a lessening of the electron beam effect as the substrate temperature increases. Comparison of the oxidation rates in Figs. 2 and 3 reveals that the electron assisted oxidation of Ni(111) at 120 K proceeds even more rapidly than in the ''electron free'' case at 250 K.

The opposite temperature dependencies of the rate of oxygen uptake for oxidation with and without an electron beam, and the similar rates of oxidation near room temperature for the two experimental conditions, must be accounted for in any consistent model of the oxidation process at this surface.

### B. Island growth model of Holloway and Hudson

Figures 4 and 5 show the data for oxidation with and without electron irradiation, fit with an oxide growth model

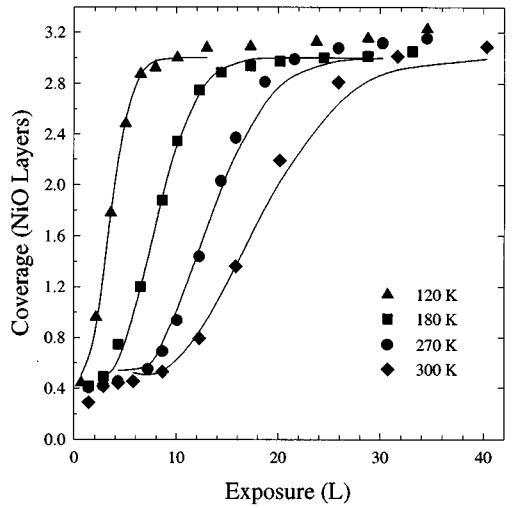


FIG. 4. Oxygen uptake vs exposure data of Fig. 2, showing nonlinear least squares fits using the island growth model [Eq. (1)].

developed by Holloway and Hudson.[4] No attempt was made to fit the data for 120 K oxidation in Fig. 5. The solid lines in that panel are fits extrapolated from fits to the three higher temperatures, using the limits of the error bars in the fitting parameter.

Holloway and Hudson proposed a model of nickel oxide growth in their original paper[4] that assumed lateral growth of circular oxide islands, based on an earlier model by Orr.[16] They considered oxidation rates limited by three different processes: the molecular oxygen impingement rate, transport of oxygen across the surface by diffusion, and the rate of

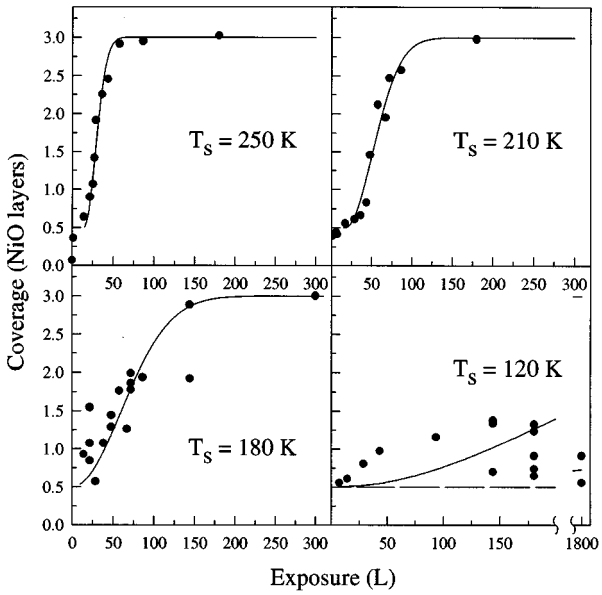


FIG. 5. Oxygen uptake vs exposure data of Fig. 3, showing nonlinear least squares fits using the island growth model [Eq. (1)]. No attempt was made to fit the data in the 120 K panel. The solid lines in that panel are predicted from the upper and lower limits of the fitting parameter obtained from the three higher temperatures, as estimated from the scatter in the experimental data.

TABLE I. Values of the fitting parameter $K[\mathrm{NiO}]_0$ obtained from fits of Eq. (1) to the electron stimulated oxidation data, compared to the values obtained in Ref. 5.

| | $K[\mathrm{NiO}]_0$ ($\mathrm{Torr}^{-2}\,\mathrm{s}^{-2}$) | |
|---|---|---|
| Surface temp. (K) | (This work) | (From Ref. 5) |
| 120 | $9.1\times10^{+10}$ | |
| 147 | | $3.9\times10^{+11}$ |
| 180 | $2.5\times10^{+10}$ | |
| 250 | $1.6\times10^{+10}$ | |
| 270 | $1.1\times10^{+10}$ | |
| 300 | $5.4\times10^{+9}$ | |
| 302 | | $8.7\times10^{+9}$ |
| 340 | $4.8\times10^{+9}$ | |
| 366 | | $2.5\times10^{+9}$ |
| 423 | | $2.0\times10^{+9}$ |

capture of oxygen at the perimeters of oxide islands. They arrived at the following expression for the observed Auger signal, $I$, as a function of the oxygen exposure, $\Phi$:

$$I(\Phi)\propto 3+([\mathrm{O}]_0-3)\exp(-K[\mathrm{NiO}]_0\Phi^2), \tag{1}$$

where $[\mathrm{O}]_0$ is the chemisorbed saturation coverage of oxygen converted to NiO layers, three layers is the saturation coverage of NiO, and $[\mathrm{NiO}]_0$ is the initial concentration of oxide, assumed to be the initial number of nucleation sites for further oxidation. This model assumes that the oxide islands only grow laterally, i.e., oxidation only occurs at the edge of a (three layer thick) oxide island. The extent of oxide growth is a function of the square of the exposure, due to the $\Phi^2$ dependence of the rate of increase in the perimeter of the oxide islands. The exponential decrease in the rate of oxide growth with exposure is a result of the coalescence of the oxide islands. The rate constant $K$ and the initial number of nucleation sites $[\mathrm{NiO}]_0$ are not separable parameters in this model, but were written in this manner by the original authors to clarify the discussion of the growth mechanism. We follow their convention here. Fitting the electron assisted oxidation curves with this model (Fig. 4) resulted in values of $K[\mathrm{NiO}]_0$ similar to those obtained by Holloway and Hudson,[5] Table I.

For the case of oxidation without an electron beam, we use the values of $K[\mathrm{NiO}]_0$ obtained from fits to the three higher temperatures and assume that the initial number of nucleation sites $[\mathrm{NiO}]_0$ is constant with decreasing surface temperature. Then, if we assume that the rate constant for oxidation, $K$, follows an Arrhenius temperature dependence, we can obtain an activation energy for oxidation without the presence of perturbing electrons. Figure 6 shows a plot of $\ln(K[\mathrm{NiO}]_0)$ vs $1/T$, from which we extract an activation energy in the island growth model for the ''intrinsic'' oxidation process of $164\pm30$ meV.

### C. Autocatalytic rate model

After oxidation of the surface to saturation, we generally used our LEED optics to get some idea of the nature of the oxide overlayer. As has been noted before for oxidation of the Ni(100) surface,[3] no NiO LEED pattern was observed for oxidation below about 130 K, while oxidation near room

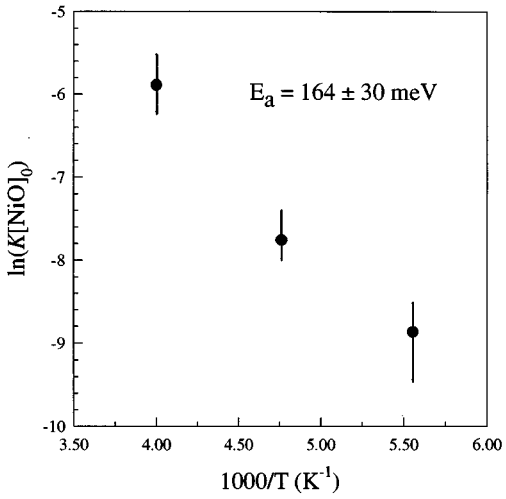


FIG. 6. Arrhenius plot of $\ln(K[\mathrm{NiO}]_0)$ vs $1/T$ using the values of $K[\mathrm{NiO}]_0$ obtained from the fits in Fig. 5. $[\mathrm{NiO}]_0$ was assumed to be temperature independent and constant in the absence of electron irradiation. The error bars are estimated from the scatter in the experimental data at the three higher temperatures shown in Fig. 5. $E_a$ is the activation energy for nickel oxidation at intrinsic nucleation sites in the island growth model.

temperature with or without an electron beam resulted in a NiO(111) LEED pattern at saturation. Furthermore, when the surface is oxidized at 120 K and subsequently annealed to 270 K, no NiO(111) LEED pattern appears. This suggests that the oxide formed at 120 K is either disordered, or consists of very small randomly oriented domains of NiO(111). In light of these observations, we believe that the rather strict requirements of the island growth model may not be an accurate representation of the oxidation mechanism on this surface, at least at these conditions, and we have developed an alternate model of the oxidation kinetics that makes no underlying assumptions about the microscopic mechanism of oxide growth.

The S-shaped curves in the oxide nucleation and growth region of Figs. 2 and 3 suggest an autocatalytic process. Accordingly, we have fit our data with a rate expression that assumes the rate of oxide growth is first order in both the concentration of existing oxide (autocatalysis), and in the concentration of chemisorbed atomic oxygen:

$$\begin{aligned} &\mathrm{O}_{(\mathrm{ads})}+\mathrm{Ni}\xrightarrow{\mathrm{NiO}}\mathrm{NiO},\\ &\frac{d[\mathrm{NiO}]}{d\Phi}=K[\mathrm{O}_{\mathrm{ads}}][\mathrm{NiO}], \end{aligned} \tag{2}$$

where $\Phi$ is the oxygen exposure in units of pressure–time. Following Holloway and Hudson,[4] we have assumed that the rate of disappearance of the chemisorbed oxygen is proportional to the rate of NiO formation:

$$[\mathrm{O}_{\mathrm{ads}}](\Phi)=[\mathrm{O}]_0\cdot\left(1-\frac{[\mathrm{NiO}](\Phi)-[\mathrm{NiO}]_0}{3-[\mathrm{NiO}]_0}\right), \tag{3}$$

where $[\mathrm{O}]_0$ is the saturation chemisorbed oxygen coverage, the equivalent of 0.4–0.5 NiO layers, $[\mathrm{NiO}]_0$ is the initial oxide coverage, and three layers is taken to be the saturation coverage of NiO. The model assumes that it is the formation of NiO (and the disappearance of the Ni adsorption sites) that limits the amount of chemisorbed oxygen atoms available to form more NiO, effectively making the rate expression first order in the factor $(3-[\mathrm{NiO}](\Phi))$. The measured Auger signal is then a combination of the Auger signal due to $[\mathrm{O}_{\mathrm{ads}}](\Phi)$, and that due to $[\mathrm{NiO}](\Phi)$, and after sufficiently long exposures, the Auger signal is entirely due to the three layers of nickel oxide. This approach was used because Auger spectroscopy at low resolution does not distinguish between the oxygen in nickel oxide and chemisorbed oxygen. Integration of the rate expression given above yields

$$[\mathrm{NiO}](\Phi)+[\mathrm{O}](\Phi)=\frac{3}{Z+1}+[\mathrm{O}]_0\left(\frac{3Z}{(3-[\mathrm{NiO}]_0)(Z+1)}\right), \tag{4}$$

where the first term is the signal due to NiO, the second term is that due to chemisorbed oxygen, and

$$Z=\frac{3-[\mathrm{NiO}]_0}{[\mathrm{NiO}]_0}\exp\left(-\frac{3[\mathrm{O}]_0}{3-[\mathrm{NiO}]_0}K\Phi\right), \tag{5}$$

where $K$ is the rate constant for oxidation. We wish to point out that for the case of electron stimulated oxidation, although we will again assume that the electron created nucleation centers are related to the initial concentration of $[\mathrm{NiO}]_0$ in the above expression, we do not yet have any information on the true nature of these sites.

In contrast to the island growth model, the two fitting parameters $K$ and $[\mathrm{NiO}]_0$ are independent in this model. Here, $[\mathrm{NiO}]_0$ governs the length of the oxidation induction period, i.e., the plateau following the initial chemisorption region, and $K$ controls the slope of the oxide formation uptake curve. Experimentally, we observe that both the induction period and the rate constant $K$ are functions of the surface temperature, both approaching the values that they have on the unirradiated surface near room temperature. Attempts to fit the data for electron stimulated oxidation with either of these parameters fixed were unsuccessful, while nonlinear least squares fits to the data with both parameters variable gave excellent fits, as shown by the solid lines in Fig. 7.

Figure 8 shows the fit of this model to the oxidation data without electron stimulation. The solid lines in the first three panels are fits to the data using the autocatalytic rate expression, and again no attempt was made to fit the uptake data for the 120 K substrate. The solid lines in that panel are the extrapolated fits predicted by the model, using the upper and lower limits of the parameters obtained from fitting the three higher temperatures. The upper and lower limits of $K$ and $[\mathrm{NiO}]_0$ were estimated from the scatter in the data in the first three panels.

Table II lists the rate constants and initial number of nucleation sites for the six substrate temperatures measured with electron irradiation, and the three temperatures without electron irradiation, that were obtained from fits to the oxidation data using this model. Note that only four of the six total uptake curves for electron assisted oxidation are plotted in Figs. 2, 4, and 7. As Table II shows, for electron assisted

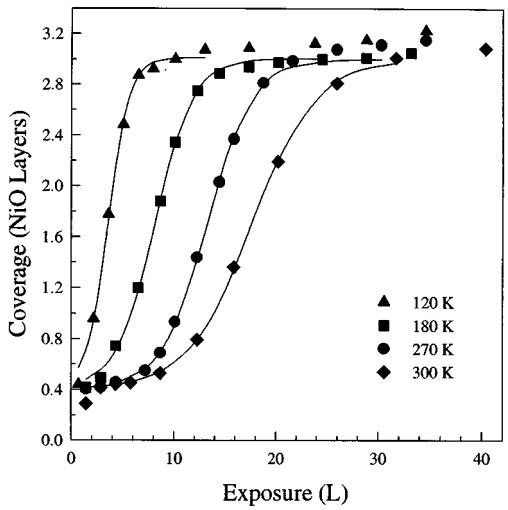


FIG. 7. Oxygen uptake vs exposure data of Fig. 2, showing nonlinear least squares fits using the autocatalytic kinetic model [Eq. (4)].

oxidation this model predicts a systematic decrease in both the rate constant and in the number of initial nucleation sites as the substrate temperature increases. For oxidation without an electron beam, the model predicts a constant value of $[NiO]_0$, and oxidation rate constants that *increase* with increasing substrate temperatures.

Figure 9 shows an Arrhenius plot of $\ln(K)$ vs $1/T$ obtained from the fits to the nonelectron assisted oxidation curves, from which we extract an activation energy of $45\pm22$ meV for the autocatalytic kinetic model. The error bars on $\ln(K)$ are estimated from the scatter in the experimental data. Again, no attempt was made to fit the data at

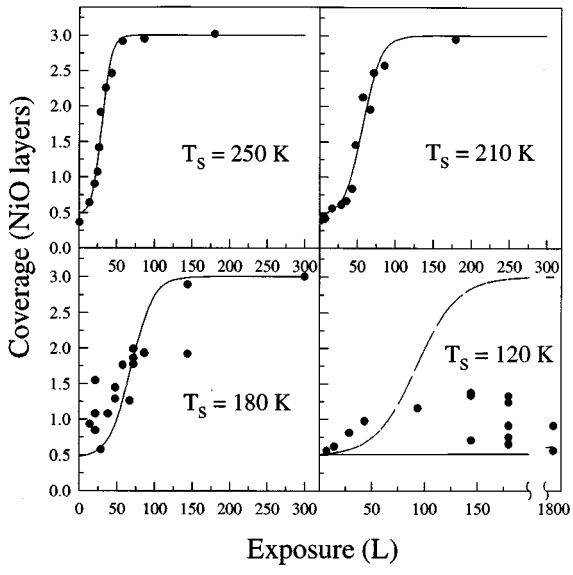


FIG. 8. Oxygen uptake vs exposure data of Fig. 3, showing nonlinear least squares fits using the autocatalytic kinetic model [Eq. (4)]. No attempt was made to fit the data in the 120 K panel. The solid lines in that panel are predicted from the upper and lower limits of the fitting parameters obtained from the three higher temperatures, as estimated from the scatter in the experimental data.

TABLE II. Values of $K$ and $[NiO]_0$ obtained from the fits of Eq. (4) to the data in Figs. 7 and 8. This model predicts that for electron stimulated oxidation both $K$ and $[NiO]_0$ are dependent on the substrate temperature.

| With electron irradiation | | | Without electron irradiation | | |
|---|---|---|---|---|---|
| Temp. (K) | $K$ (layer$^{-1}$ L$^{-1}$) | $[NiO]_0$ (layers) | Temp. (K) | $K$ (layer$^{-1}$ L$^{-1}$) | $[NiO]_0$ (layers) |
| 120 | 2.39 | 0.087 | 180 | 0.154 | 0.024 |
| 180 | 1.33 | 0.038 | 210 | 0.185 | 0.024 |
| 250 | 1.21 | 0.010 | 250 | 0.347 | 0.025 |
| 270 | 1.12 | 0.008 | | | |
| 300 | 0.80 | 0.010 | | | |
| 340 | 0.81 | 0.007 | | | |

120 K substrate temperature. Comparison of the activation energy predicted by this model with that predicted by the island growth model shows that this model predicts a much lower activation energy, a consequence of the first order dependence of the growth rate on the concentration of oxide.

### D. Stability of electron created nucleation centers

As was shown in our original study,[6] it is not necessary to have simultaneous electron and oxygen exposure to oxidize the surface at low temperatures. In fact, a single large dose of electrons from the Auger gun (2 keV, 2.00 mA cm$^{-2}$, 20 s) on the chemisorbed oxygen overlayer at 120 K will result in oxidation to saturation upon subsequent exposure of the surface to oxygen. It was noticed, however, that the extent of oxidation for a fixed oxygen dose depended on how long one waited between the end of the electron dose and the start of the oxygen dose. Figure 10 shows this effect graphically for two substrate temperatures, 120 and 180 K. The data were obtained in the following manner: The crystal was first exposed to a fixed amount of oxygen, $3\times10^{-8}$ Torr, for 10 min at 120 K and for 5 min at 180 K. A spot on the

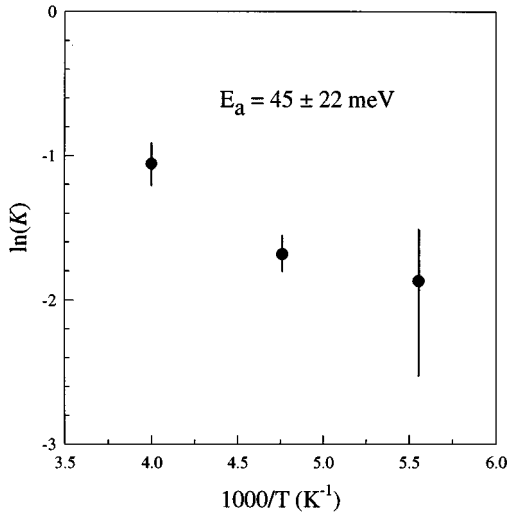


FIG. 9. Arrhenius plot of $\ln(K)$ vs $1/T$ for oxidation without electron irradiation, using values of $K$ obtained from the fits in Fig. 8. The error bars are estimated from the scatter in the experimental data. $E_a$ is the activation energy for nickel oxidation at intrinsic nucleation sites in the autocatalytic model.

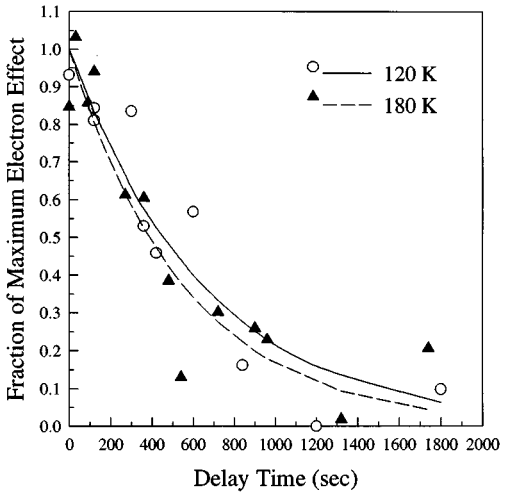


FIG. 10. Plot demonstrating the time decay of the electron beam effect as described in the text. The solid lines are nonlinear least squares fits to the data using an exponential decay rate expression. From these fits the half-life of the electron beam created nucleation centers is determined to be $10\pm2$ min.

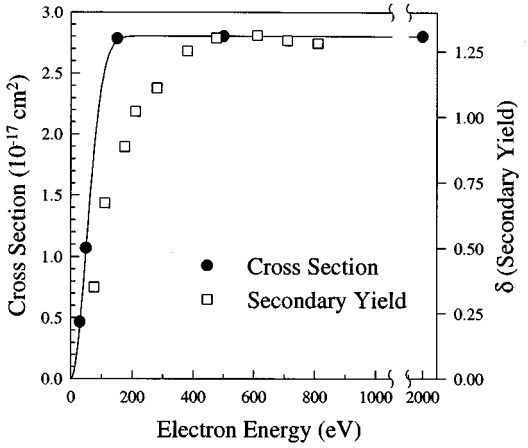


FIG. 11. Dependence of the cross section for the creation of nucleation centers on the energy of the incident electron beam (solid circles). The solid line is a curve drawn to guide the eye. The open squares are data for the number of secondary electrons emitted from polycrystalline evaporated nickel films per incident primary electron ($\delta$) as a function of primary electron energy (from Ref. 17).

crystal was then exposed to a standard dose of electrons from the Auger electron gun (see above), and a fixed period of time was allowed to elapse before a second dose of oxygen at $3\times10^{-8}$ Torr for 10 min. After all oxygen had been pumped from the chamber, the extents of oxidation in the spot exposed to the electron beam and in an area that had not been exposed to the electron beam were assessed with Auger spectroscopy. The percent of the total uptake that was due to the electron beam was determined from

$$\text{Fraction}_{e\text{-beam}}=\frac{[\text{NiO}]_{e\text{-beam}}-[\text{NiO}]_{\text{background}}}{[\text{NiO}]_{e\text{-beam}}}, \tag{6}$$

where $[\text{NiO}]_{e\text{-beam}}$ is the oxidation extent in the $e$-beam spot and $[\text{NiO}]_{\text{background}}$ is the oxidation extent on the rest of the crystal, as determined from Auger intensities. The fraction vs delay time data were fit with simple exponential decay expressions (solid and dashed lines), and then the data and fits for each temperature were normalized to the maximum electron beam effect at that temperature (i.e., at 0 delay time). The normalization procedure accounts for the differing oxidation kinetics at the two temperatures. From the fits to the data we obtain a fairly temperature independent half-life for the electron created nucleation centers of about 10 min.

### E. Incident electron energy dependence

Figure 11 shows a more detailed investigation of the experimentally determined cross sections for electron assisted oxidation as a function of incident electron energy. The cross sections were determined by fitting oxygen uptake vs electron flux at constant oxygen exposure data with an expression that has been derived previously:[6]

$$[\text{NiO}](t)=3-(3-[\text{NiO}]_{\text{chem}})\times\exp\left(-K\left(t+\frac{1}{\phi_e\sigma}\exp(-\phi_e\sigma t)-\frac{1}{\phi_e\sigma}\right)\right), \tag{7}$$

where $t$ is the electron beam exposure time, $K$ is the rate constant for oxidation, $[\text{NiO}]_{\text{chem}}$ is the chemisorbed saturation coverage of oxygen converted to layers of NiO, $\phi_e$ is the electron beam current density, and $\sigma$ is the cross section for creation of the nucleation centers by the electron beam, the only adjustable parameter. This expression was found to give an excellent fit to both the uptake vs electron flux data and oxygen uptake vs oxygen exposure data over 2 orders of magnitude variations in electron flux.

The cross sections saturate in the region of 100 eV electron energy, and constant cross sections are obtained above this energy, out to 2 keV. Also plotted in Fig. 11 is the yield of secondary electrons obtained per incident primary electron for the same range of incident electron energies, obtained from polycrystalline evaporated nickel films.[17] The implications of the similarity in the two curves is discussed below.

## IV. DISCUSSION

We have shown that our kinetic oxidation data can be fit reasonably well using an island growth kinetic model, which approximates the oxide growth by the lateral growth of three layer high circular islands. We now examine the conclusions about the electron stimulated oxidation process that can be drawn from this model by comparing fits for electron stimulated and nonelectron stimulated oxidation. As was shown in Fig. 6, the temperature dependence of the rate constant $K$ can be extracted from fits to the oxidation data without electron irradiation by assuming that $[\text{NiO}]_0$ is constant over this temperature range. Because $K$ and $[\text{NiO}]_0$ are not independently variable in this model, the faster rates at lower temperature for electron assisted oxidation, where $K$ is assumed to de-

crease with temperature as in the nonassisted oxidation experiment, can be accounted for by a corresponding increase in $[NiO]_0$. To test this hypothesis, we assume that $K$ has the same temperature dependence for the case of electron assisted oxidation as for nonelectron assisted oxidation (where $[NiO]_0$ was assumed to be temperature independent), and the approximate temperature dependence of $[NiO]_0$ in the presence of the electron beam is extracted from a plot of $\ln(K[NiO]_0)$ vs 1/T. Using this method, we find that $[NiO]_0(T)$ grows as approximately exp(2400/T). From this we see that assuming that it is only the greater number of nucleation sites at lower temperatures that produces the much faster oxidation rates with electron irradiation requires on the order of a $10^5$ increase in the concentration of nucleation sites in going from a 300 K surface to a 120 K surface, and continuing the same trend, would require a factor of $10^{10}$ increase in nucleation site density in going from 300 to 77 K. Taking the maximum number of nucleation sites as the number of nickel sites on the clean surface, on the order of $10^{15}$ $cm^{-2}$, and if $[NiO]_0$ were to saturate at 77 K, then this argument predicts only about $10^5$ nucleation sites per $cm^2$ on the surface at 300 K, which is probably several orders of magnitude lower than the intrinsic defect density of this surface. From this reasoning, it appears unlikely that it is only an increase in the number of nucleation sites that causes the faster rates of oxidation at lower temperatures. On the other hand, if we assume that the rate constant $K$ is larger for electron beam created nucleation sites than for intrinsic sites, then the increase in the relative population of the electron beam created nucleation sites at lower temperatures would result in an apparent increase in the overall oxidation rate. Alternatively, we can imagine that the rate constant $K$ is dependent on the concentration of nucleation sites, and it is the morphology of the oxide growth at a high density of nucleation sites that increases the value of the rate constant. In fact, the absence of a NiO LEED pattern at low temperatures suggests the possibility of a high density of randomly oriented oxide domains. In either case, it appears that this model predicts an increase both in $K$ and in $[NiO]_0$ with a decrease in substrate temperature for electron stimulated oxidation.

We have also shown that the kinetics of oxidation of the Ni(111) surface can be described very well using an autocatalytic rate expression. As was stated previously, the autocatalytic kinetic model afforded good fits to the data only when the two parameters, $[NiO]_0$ and $K$, were allowed to vary independently. This resulted in both parameters exhibiting inverse temperature dependencies below 250 K (Table II). Inspection of Table II reveals that this model explicitly predicts an increase in the rate constant $K$ as the substrate temperature is lowered during electron stimulated oxidation. Moreover, comparing the results of this model in the case of electron beam assisted oxidation with those for nonassisted oxidation, where $K$ **increased** with increasing substrate temperature and $[NiO]_0$ was constant, it appears that this model predicts that the rate constant $K$ is an increasing function of the nucleation site density $[NiO]_0$, again suggesting that interactions may exist between nucleation sites which are dependent on the proximity and density of such sites.

As before, if the electron beam creates nucleation sites that have a lower barrier to oxidation than intrinsic nucleation sites, and/or are capable of reacting with more adsorbed oxygen than intrinsic sites, then the increasing number of these easily oxidizable sites would indeed be reflected in an apparent increase of the rate constant $K$ with $[NiO]_0$. As a reminder, we have shown that it is possible to oxidize the 120 K surface with approximately the same kinetic behavior by using a single finite dose of electrons on the chemisorbed oxygen overlayer followed by oxygen exposure, which precludes the possibility that continuous creation of nucleation sites by the electron beam during the course of the oxidation is responsible for the kinetic temperature dependence. A final experiment was run to verify the proposal that $K$ is dependent on $[NiO]_0$ and not surface temperature: The surface was first exposed to oxygen at 120 K to the chemisorbed saturation limit. The surface was then dosed with 2 keV electrons at 2.00 mA $cm^{-2}$ for 20 s. The sample was then quickly heated to 270 K and dosed with oxygen to saturation while monitoring the uptake with Auger spectroscopy, during which time it was observed that *the oxidation followed the 120 K kinetics, and not the 270 K kinetics*. This experiment clearly shows that in the case of electron stimulated oxidation, *it is the temperature at which the electron beam creates the nucleation sites that determines the kinetics of oxidation, and not the temperature at which the oxidation takes place.*

This autocatalytic model can be directly compared to the model of oxide growth proposed in Ref. 6. In that paper, we proposed a rate expression that was first order in the number of nucleation sites, and first order in the saturation coverage of nickel oxide:

$$\frac{d[\mathrm{NiO}]}{d\Phi} = K(3-[\mathrm{NiO}])\cdot\frac{[\mathrm{N}](t)}{[\mathrm{N}]_{(\max)}}. \tag{8}$$

In that series of experiments, we varied the rate of nucleation site creation, $[N](t)$, by varying the flux of incident electrons from 2.00 mA $cm^{-2}$ to as low as 1.3 $\mu$A $cm^{-2}$. In order to see any change in the oxidation kinetics, the electron flux had to be reduced from 2.00 mA $cm^{-2}$ to 9.8 $\mu$A $cm^{-2}$. In contrast, in the present experiment, we have used the constant very high flux of electrons at 2.00 mA $cm^{-2}$ to quickly saturate the initial (temperature dependent) number of nucleation sites at $[N]_{(max)}$. (From our measured cross sections at this flux, this takes on the order of 3 s.) As a result, we have approximated the second factor in Eq. (8) as unity in our new rate expression. In addition, because the previous experiments were done at a constant temperature of 120 K, where the rate constant $K$ was large, we could neglect the second order effect of the oxide coverage on the rate, an effect that has been included here. In short, in this work we have explored a regime where the kinetics of oxidation were dominated by autocatalysis effects, and in the previous paper we explored the regime where the kinetics were dominated by the creation rate of the nucleation sites.

Some insight on the nature of the oxygen reaction with the nucleation sites, which we have assumed to be some form of $Ni_xO_y$, can be obtained from work done on the interaction of oxygen with NiO and with thin films of NiO

grown on Ni surfaces.[18–26] Most authors agree that oxygen adsorption on NiO requires the presence of defect sites, however, there is some disagreement on the nature of the adsorbed oxygen species. McKay and Henrich attributed oxygen uptake on cleaved NiO(100) to adsorption of an $O^{2-}$ species at anion vacancies that had been created by sputtering.[21,22] In contrast, Bushby *et al.*[26] have used the thermal desorption of mixed isotopes to convincingly demonstrate that oxygen adsorbs molecularly on thin films of oxide grown on Ni(100) and (110). The majority of defects in oxide layers grown on Ni surfaces are believed to be $N_2O_3$, the so-called defect oxide. This species is concentrated at the surface of epitaxial films, and may comprise as much as 70% of the surface oxide.[27] A third type of defect in epitaxially grown NiO is the impurity defect, and several studies have shown that oxygen adsorption on NiO is enhanced by the presence of surface OH groups.[21,22,24]

Although these studies are not directly applicable to the incipient oxidation of the Ni(111) surface, it appears clear that the oxidation sites created by the electron beam are not $Ni_2O_3$ defect sites. These sites are quite prevalent on the room temperature oxide, and oxygen is believed to adsorb molecularly at these sites.[26] It seems more likely that these electron created nucleation sites are some type of electron rich site, similar to the $f$-center anion vacancies created by sputtering the NiO surface. It is these sites that have shown evidence of the dissociative adsorption of $O_2$. In fact, we have also observed facile oxidation of surfaces roughened by $Ar^+$ sputtering. The use of a source of atomic oxygen, such as an atomic oxygen beam or the use of a reagent that easily delivers O atoms to the surface, such as $NO_2$, would help to clarify the role of molecular vs atomic oxygen in the oxidation of this surface.

A final possible cause of this effect is the electron impact dissociation of adsorbed water to form surface OH groups, which catalyze the oxidation of the surface. While this mechanism is consistent with the temperature dependence of the nucleation site density, at $2\times10^{-11}$ Torr (a conservative estimate of the background partial pressure of water in our chamber), it would take on the order of 1 h to adsorb the 0.08 ML of water necessary to account for the calculated density of nucleation sites. Further, the oxidation kinetics were not dependent on the cool down time of the crystal, or whether the crystal was flashed and quickly recooled prior to dosing or not. Finally, we observe the electron beam effect only after irradiation of an oxygen covered surface, and not after irradiation of the clean surface.

Two final considerations are the observed decay of the electron created nucleation centers and the saturation of the cross section near 100 eV incident electron energy. The half-life of the decay rate, $10\pm2$ min, is much too long for the electron created nucleation sites to be considered as any of the usual excited states of surface adsorbates, such as negative ion resonances or excited electronic states. (The length of this half-life suggests the possibility of reaction with background gases as a cause in the disappearance of the electron beam created nucleation centers. For example, reduction of electron beam created oxide sites by background hydrogen could be a factor.) This again points to some relatively stable nickel–oxygen surface species. It is our opinion that these nucleation sites are a reconstruction of the surface in which an oxygen atom is incorporated into the nickel lattice. The saturation in the cross section at about 100 eV may be related to the number distribution of secondary electrons emitted by a metal under electron irradiation, which also shows a similar energy dependence in this incident energy range, as shown in Fig. 11. In fact, it could be argued that the creation of a surface negative ion by electron attachment to an adsorbed oxygen species is an intermediate in the creation of the nucleation sites. Electron attachment would be most efficient for electrons near 1 eV energy, such as the swarms of low energy secondaries emitted from a metal surface under electron bombardment. Because the NiO(111) surface is polar, attachment of an electron to an adsorbed oxygen atom or molecular could facilitate its transport through the surface charge separation and permit its incorporation as an oxide. However, if the disappearance rate of the nucleation centers is due to self-annealing of this electron beam stimulated reconstruction, it would be expected to exhibit a temperature dependent half-life. Due to the uncertainty in our measurement and the limited temperature range investigated we were unable to determine if this was so.

A final word on the physical mechanisms underlying the two kinetic models: the first order autocatalytic rate expression makes no assumptions as to the spatial dependence of the oxide growth, but its first order kinetics could be accounted for by a number of physical mechanisms, e.g., dendritic growth of the oxide at nucleation sites or some other complex morphology. On the other hand, the island growth model begins with the rather rigid stipulation that the (already three layers thick) oxide islands grow only laterally at their edges. The actual growth mechanism is probably closer to a combination of these two models. At higher substrate temperatures, when the nucleation site density is low, the island growth kinetic model may be more accurate, while at lower temperatures, with a high density of nucleation sites, a more complex growth model may be more accurate. Atomic resolution microscopy experiments will be a logical follow-up to these measurements.

## V. CONCLUSION

In conclusion, we have demonstrated that two independent kinetic models predict that both the rate constant for electron assisted oxidation and the number of nucleation sites created by the electron beam are increasing functions of decreasing substrate temperatures. This apparent increase in the rate constant we attribute to different relative populations of two types of oxide nucleation sites at different temperatures. One type of nucleation site is intrinsic to the surface, and possesses a larger activation energy than the other site, which is created by electron irradiation of a chemisorbed oxygen overlayer. These electron created nucleation sites are metastable, with a half-life of about 10 min, precluding their assignment as excited electronic states or surface negative ion resonances. The sites may be some form of electron rich NiO, and their creation may be related to the emission of

secondary electrons, which shows a similar incident electron energy dependent threshold to that observed for the cross section of electron stimulated oxidation.

We have also reported on the true intrinsic low temperature oxidation kinetics for Ni(111), i.e., the correct behavior without the perturbing influence of electron irradiation, and have shown that in this case the rate constant decreased with decreasing substrate temperature, falling almost to zero at 120 K. We have obtained estimates of the activation energies from both kinetic models from the oxidation rate constants.

The results presented herein clarify several puzzling trends that have persisted in the literature for metallic oxidation for quite some time. They also provide a cautionary note for experiments which use electron-based probes, or optical probes which generate intense swarms of secondary electrons, for studying the oxidation kinetics of metals, and perhaps other classes of interfacial reactions.

## ACKNOWLEDGMENTS

We would like to thank Jennifer Colonell and Kevin Gibson for many helpful discussions. This work was supported by the Air Force Office of Scientific Research, and, in part, by the MRSEC Program of the National Science Foundation under Award Number DMR-9400379.

[1] P. R. Norton, R. L. Tapping, and J. W. Goodale, Surf. Sci. **65**, 13 (1977).
[2] T. M. Christensen, C. Raoul, and J. M. Blakely, Appl. Surf. Sci. **26**, 408 (1986).
[3] W. -D. Wang, N. J. Wu, and P. A. Thiel, J. Chem. Phys. **93**, 2025 (1990).
[4] P. H. Holloway and J. B. Hudson, Surf. Sci. **43**, 123 (1974).
[5] P. H. Holloway and J. B. Hudson, Surf. Sci. **43**, 141 (1974).
[6] Wei Li, M. J. Stirniman, and S. J. Sibener, Surf. Sci. Lett (to be published).
[7] Wei Li, M. J. Stirniman, and S. J. Sibener, J. Vac. Sci. Technol. A (to be published).
[8] C. Xu and B. E. Koel, Surf. Sci. **292**, L803 (1993).
[9] R. Ramsier and J. T. Yates, Jr., Surf. Sci. Rep. **12**, 243 (1991).
[10] J. H. Jänsch, J. Xu, and J. T. Yates, Jr., J. Chem. Phys. **99**, 721 (1993).
[11] W. Menezes, P. Knipp, G. Tisdale, and S. J. Sibener, Phys. Rev. B **41**, 5628 (1990).
[12] Jun Liu, J. P. Lu, P. W. Chu, and J. M. Blakely, J. Vac. Sci. Technol. A **10**, 2355 (1992).
[13] A. R. Kortan and R. L. Park, Phys. Rev. B **23**, 6340 (1981).
[14] D. E. Taylor and R. L. Park, Surf. Sci. **125**, L73 (1983).
[15] S. Reindl, G. M. Pastor, and K. H. Bennemann, Surf. Sci. **211/212**, 912 (1989).
[16] W. H. Orr, Thesis, Cornell University, Ithaca, NY, 1962.
[17] D. E. Woolridge, Phys. Rev. B **56**, 1063 (1939).
[18] A. A. Tsyganenko, T. A. Rodionova, and V. M. Filimonov, React. Kinet. Catal. Lett. **11**, 113 (1979).
[19] M. W. Roberts and R. St. C. Smart, Surf. Sci. **108**, 271 (1981).
[20] J. M. Blaisdell and A. B. Kunz, Phys. Rev. B **29**, 988 (1984).
[21] J. M. McKay and V. E. Henrich, Phys. Rev. B **32**, 6764 (1985).
[22] J. M. McKay and V. E. Henrich, J. Vac. Sci. Technol. A **5**, 722 (1987).
[23] S. P. Mehandru and A. B. Anderson, J. Electrochem. Soc. **133**, 828 (1986).
[24] E. Escalona Platero, G. Spoto, S. Coluccia, and A. Zecchina, Langmuir **3**, 291 (1987).
[25] V. M. Allen, W. E. Jones, and P. D. Pacey, Surf. Sci. **220**, 193 (1989).
[26] S. J. Bushby, T. D. Pope, B. W. Callen, K. Griffiths, and P. R. Norton, Surf. Sci. **256**, 301 (1991).
[27] M. W. Roberts and R. St. C. Smart, J. Chem. Soc. Faraday Trans. 1 **80**, 2957 (1984).